The effect of morphology upon mobility: Implications for bulk heterojunction solar cells with nonuniform blend morphology

C. Groves,[a] L. J. A. Koster, and N. C. Greenham
Cavendish Laboratory, J. J. Thomson Avenue, Cambridge, CB3 0HE, United Kingdom

(Received 5 January 2009; accepted 15 March 2009; published online 13 May 2009)

We use a Monte Carlo model to predict the effect of composition, domain size, and energetic disorder upon the mobility of carriers in an organic donor-acceptor blend. These simulations show that, for the changes in local morphology expected within the thickness of a typical bulk heterojunction photovoltaic device, changes in mobility of more than an order of magnitude are expected. The impact of nonuniform mobility upon space-charge-limited diode and photovoltaic (PV) device performance is examined using a drift-diffusion model. The current passing through a space-charge-limited diode is shown to depend upon the position of the layers with differing mobility. Accurate modeling of the current in such devices can only be achieved using a drift-diffusion model incorporating nonuniform mobility. Inserting a 20 nm thick layer in which the mobility is less by one order of magnitude than in the rest of the 70 nm thick PV device reduced the device efficiency by more than 20%. Therefore it seems vital to exert a high degree of control over the morphology throughout the entire blend PV device, otherwise potential PV performance may be lost. © *2009 American Institute of Physics*. [DOI: 10.1063/1.3117493]

I. INTRODUCTION

Solution-processable materials are attractive candidates for photovoltaic (PV) devices because of their potential low cost. However, such materials typically have a high exciton binding energy and require films of thickness ~100 nm to efficiently absorb light. Consequently, to have viable charge generation one must use an intimately mixed blend of donor and acceptor materials, the heterojunctions between which drive exciton dissociation.[1,2] Such bulk heterojunctions (BHJs) are easily realized by blending the donor and acceptor materials in solution prior to deposition. Unfortunately, the constraints placed on the morphology by charge generation, which is favored by a fine phase separation, are counter to those of charge transport, which is favored by a coarse phase separation. Consequently, balancing the competing demands upon the morphology is critical to optimizing PVs. Many methods exist to alter the morphology of a BHJ, including annealing,[3] and the choice of solvent[4] or cosolvent.[5] However, while these techniques broadly control the domain size, crystallinity, or packing of the components of the BHJ, these characteristics of the blend morphology are not uniform throughout the film. Indeed, studies of the structure of polymer-polymer,[3,6,7] polymer-fullerene,[8–10] and polymer-nanocrystal[11] blends show hierarchies of phase separation and vertical variations in the blend morphology. How this local variation in blend morphology affects the local mobility of carriers, and in particular the PV performance, is largely unknown. This may be a serious deficiency in our knowledge, especially since the limited existing studies point to significant changes in charge transport when some aspects of morphology are changed.[12–16] In particular, Frost *et al.*[12] showed that networks of self-repelling and self-attracting polymers show orders of magnitude difference in mobility and substantially different dispersive character.

In this paper we use a Monte Carlo model to reveal the dependence of mobility upon domain size, blend composition, and energetic disorder. It is predicted that local changes in the characteristics of blend morphology seen in high-performance PV devices can lead to local changes in the mobility by more than an order of magnitude. The effect of nonuniform mobility upon space-charge-limited (SCL) diode and PV device performance is then investigated using a drift-diffusion model. The current passing through SCL diodes is found to be sensitive not only to the local mobility variations, but also to where within the device the variations occur. This shows that caution should be exercised when deriving SCL mobility from devices with nonuniform blend morphology. PV device performance is also shown to be significantly affected by nonuniform mobility, indicating that good morphology control is vital if one is not to lose potential performance. Furthermore it is shown that models, which assume the blend to be a homogeneous effective medium, are not capable of reproducing well the performance of a PV device with nonuniform mobility. We conclude that it is important to experimentally characterize and control the blend morphology throughout the film and to develop models that can take into account the local variations in mobility, which are a consequence of nonuniform blend morphology.

II. THE EFFECT OF MORPHOLOGY UPON LOCAL MOBILITY

First, we shall examine the effect of morphology upon mobility using a Monte Carlo model. Here we represent the morphology as a regular 1 nm Cartesian lattice comprising donor and acceptor sites extending 70 nm in each direction. Initially, the sites are chosen at random to be either donor or acceptor in accordance with the ratio of the acceptor volume

[a]Electronic mail: cg378@cam.ac.uk.

TABLE I. Parameters used in the Monte Carlo simulations.

Disorder (meV)	ν_{hop} (s^{-1})	E_R (J)
0	3×10^{9}	4×10^{-20}
100	1.1×10^{12}	4×10^{-20}
125	5×10^{13}	4×10^{-20}

to total volume, α. Thereafter, the simulated annealing approach of Peumans *et al.*[17] is used to coarsen blend as required. In summary, this technique involves choosing a pair of neighboring sites at random and probabilistically admitting a swap based on the energy change of the system.[14,15,17] Note that since cyclic boundary conditions are allowed for transport (see later), pairwise swaps over matching faces of the morphology are also allowed. Phase separation is encouraged by choosing the interfacial energies of the acceptor (E_{DD}), acceptor (E_{AA}), and heterojunction (E_{AD}) such that $2E_{AD}=E_{AA}=E_{DD}$. Boltzmann factors are included to satisfy detailed balance. During the succession of annealing steps, the domain size of the minority component is calculated from

$$d=\frac{6\beta V}{A}, \tag{1}$$

where A is the interfacial area, V is the total blend volume, and β is the volume fraction of the minority component (i.e., $\beta=\alpha$ when $\alpha\leq0.5$, $\beta=(1-\alpha)$ when $\alpha>0.5$). Note that we create at least 50 morphologies, which share the same characteristics (d and α) to ensure that we are sampling the average behavior for a particular type of morphology. Thereafter, this set of morphologies is used in a Monte Carlo model to predict mobility in a manner similar to that reported previously.[14,16] In summary, each site is assigned a Gaussian distributed energetic disorder of standard deviation σ prior to each simulation, and then an electron is placed on an acceptor site at random. The rate of hopping between the current site (i) and a nearest neighbor site (j) is calculated using a Marcus rate expression,

$$R_{i\rightarrow j}=\nu_{hop}\exp\left[-\frac{(E_j-E_i+E_r)^2}{4E_rk_BT}\right], \tag{2}$$

where E_i and E_j are the energies of the sites i and j, respectively, and E_r is half the polaron relaxation energy. The energies of the sites include energetic disorder and the applied electric field $F=10^5$ V/cm in all cases. The parameters used in Eq. (2) are chosen to give a low-field mobility of 10^{-4} cm^2/Vs, and are shown in Table I. Hops are only allowed between acceptor sites. Hop times are generated from $\tau_{i\rightarrow j}=-\ln(X)/R_{i\rightarrow j}$, where X is a random number between 0 and 1, and the process with the shortest wait time is chosen as the behavior for the carrier. The mobility is calculated from $\mu=x/Ft$, where x is the distance traveled downfield in time t. Since carriers are injected at random points within the lattice, their initial energy distribution matches the density of states rather than the equilibrium energy distribution,[18] and consequently their mobility is transiently enhanced. Since carriers are expected to thermalize rapidly within the density of states, the experimentally relevant variable is the equilibrium mobility. Hence, we measure mobility as a function of time and only record the time-independent mobility corresponding to equilibrated carriers. Note that we are examining low charge densities typically found in time-of-flight experiments and PV devices under normal operating conditions. The process is then repeated with different conformations of energetic disorder and morphology (all with the same d and α) to ensure accurate sampling of average behavior.

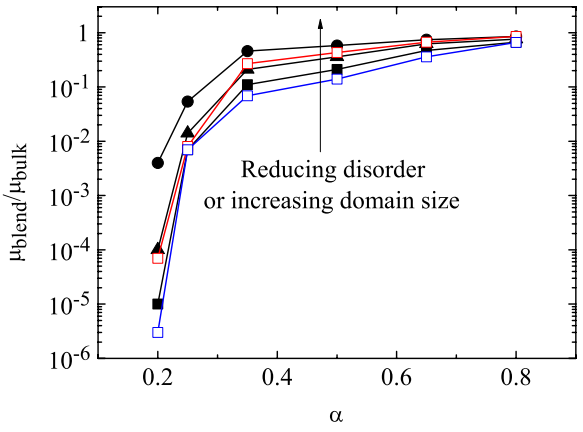

FIG. 1. (Color online) The ratio of electron mobility in the blend μ_{blend} to that in the bulk μ_{bulk} as a function of volume fraction of the acceptor material to the total volume α. Squares, triangles, and circles represent blends with d=4, 8, and 12 nm, respectively. Energetic disorder is either σ=0 (red), 100 meV (black), or 125 meV (blue). Lines are a guide to the eye.

Figure 1 shows the ratio of the mobility of electrons in the blend, μ_{blend}, to that in the bulk, μ_{bulk}, for 4 nm$\leq d\leq$12 nm, $0\leq\sigma\leq125$ meV, and $0.2\leq\alpha\leq0.8$. All of the curves show the same general character, with μ_{blend}/μ_{bulk} dropping as α reduces, simply as a consequence of there being fewer acceptor pathways for the electrons through the morphology. Figure 1 shows that μ_{blend} drops precipitously when α reduces below 0.25; indeed, for all cases examined μ_{blend} is one order of magnitude less than μ_{bulk} when $\alpha=0.25$.

Domain size and energetic disorder are also shown to have a significant effect upon μ_{blend}. Note that it is the domain size of the minority component that defines each morphology curve on Fig. 1. Hence, when $\alpha<0.5$, electrons are traveling *through* a network of domains of size d, and when $\alpha>0.5$, electrons are traveling *around* a network of domains of size d. First considering $\alpha<0.5$, Fig. 1 shows that carrier mobility is improved when the domain size of the transporting component is increased, as would be expected.[12] When $\alpha>0.5$, Fig. 1 shows that carrier mobility is reduced when the domain size of the nontransporting component is reduced. Reducing the domain size when $\alpha>0.5$ implies that the nontransporting component is better dispersed through the transporting component. This in turn impedes transport more effectively and so the mobility is reduced. Interestingly, increasing the degree of energetic disorder is shown to reduce μ_{blend}/μ_{bulk} for a given morphology, i.e., the energetic disorder has a larger effect on the mobility in the blend than it does in the bulk. Increasing the degree of energetic disorder naturally creates pathways where transport is, or is not, energetically favored, with the former being termed

filaments.[19] In essence, filaments are an energetic landscape through which carriers have to negotiate in much the same way that the BHJ is a physical landscape for carriers to negotiate. For efficient transport one would want these two networks to be coincident, however, in this model, the position of the filaments bears no relation to the physical morphology and so the mobility is reduced. Since guiding along filaments improves as σ/k_BT increases, $\mu_{\text{blend}}/\mu_{\text{bulk}}$ reduces as the degree of energetic disorder increases for a given morphology.

Hence we have shown that local blend morphology can cause orders of magnitude reduction in the mobility when $\alpha<0.25$. It is important to realize at this point that the blend morphologies in regions of some PV devices access this regime. Indeed, even high-performance polymer:polymer PVs have been shown to have strata with $\alpha=0.15$,[3] which according to Fig. 1, would give many orders of magnitude reduction in the local mobility. We now use a drift-diffusion model to give some insight into how nonuniform blend morphology, and the mobility variations it causes, affects device performance.

III. MOBILITY VARIATIONS IN SCL DIODES

As a first step, we examine the effect of nonuniform mobility upon SCL diodes. This is important since current-voltage measurements on SCL diodes are often used to characterize the mobility of carriers in a blend, and so help interpret PV performance.[20,21] Here we consider devices with a layer in which the electron mobility is one order of magnitude lower than in the rest of the device (in which $\mu_e = 10^{-10}$ $\text{m}^2/\text{V s}$). For simplicity we ignore the dependence of the mobility on field and carrier density, which is discussed in detail in Ref. 22. Note that one order of magnitude variation in mobility is well within the variation in mobility expected in some real devices. Two types of devices are considered: Case I, in which the low-mobility region is adjacent to the cathode and Case II, in which the low-mobility region is adjacent to the anode. The thickness of the low-mobility layer z is allowed to vary from zero to the device thickness $L(=70$ nm).

The current-voltage characteristics of single-carrier devices are predicted by self-consistently solving the Poisson and drift-diffusion equations,[20] while suppressing hole injection. Here we assume both contacts are electron-injecting (Ohmic), although we note that the behavior shown does not change if the anode is assumed to be noninjecting and a perfectly absorbing boundary. The parameters used in this simulation are given in Table II. In both cases reducing the mobility reduces the current as expected. Our results are very similar to those of Crone *et al.*,[23] who examined the consequence of a Case I type structure for light-emitting diodes. In the context of PV devices, SCL diodes are important because they are often used to derive mobilities for carriers within blend morphologies. Hence, we now interpret the resultant current-voltage curves using a model, which assumes a uniform blend morphology, as in Refs. 20 and 21, to determine the effective electron mobility $\mu_{e,\text{eff}}$ for the device with a nonuniform blend morphology. The results shown in Fig. 2(a) indicate that the insertion of a layer with an electron mobility that is one order of magnitude lower than in the rest of the device is detrimental to the transport through the whole of the device. For Case I, just 10 nm is sufficient to reduce $\mu_{e,\text{eff}}$ by a factor of four, whereas the implications for Case II are less dramatic because the electron concentration is greatest adjacent to the cathode. Clearly the position of the low mobility layer is important in determining the current in a SCL diode, and in turn the effective mobility. The mobility one derives from a nonuniform device is therefore not a good indicator of charge transport processes. However, it would be preferable if one did not have to use a drift-diffusion model, which incorporates nonuniform mobility to interpret data from nonuniform devices. Consequently, we have rederived the Mott–Gurney law to determine the effective mobility for a device with nonuniform mobility (for full derivation see Appendix). By setting the mobility to be μ_1 over the range 0 to z and μ_2 elsewhere, we find the effective mobility to be

$$\mu_{\text{eff}} = \left\{ \frac{1}{\sqrt{\mu_1}}\left[\frac{3}{2}\sqrt{\frac{z}{L}} - \frac{1}{2}\left(\frac{z}{L}\right)^{3/2}\right] + \frac{1}{\sqrt{\mu_2}}\left(1-\frac{z}{L}\right)^{3/2}\right\}^{-2}. \tag{3}$$

The predictions of Eq. (3) for Case I and Case II are shown in Fig. 2. It can be seen that Eq. (3) underestimates the effective mobility for both Cases I and II. Hence, even when

TABLE II. Parameters used in the drift-diffusion simulations. The parameter a is the initial separation of the geminate pair, while k_f is the recombination rate of a geminate pair to ground (Ref. 23).

Quantity	Value
relative dielectric constant	2.1
hole mobility	10^{-7} $\text{m}^2/\text{V s}$
electron mobility (bulk)	10^{-10} $\text{m}^2/\text{V s}$
bound pair generation rate	5×10^{27} $\text{m}^{-3}\ \text{s}^{-1}$
k_f	10^5 s^{-1}
a	1.5 nm
built-in voltage	1.6 eV

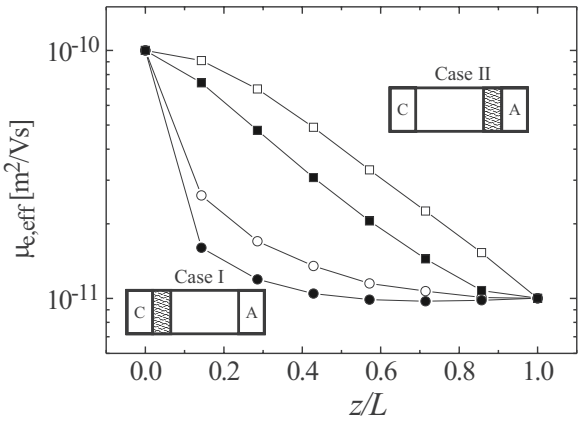

FIG. 2. Simulated (open symbols) and analytical (closed symbols) results for the effective electron mobility as a function of the fraction of the device comprising the lower mobility, z/L. Case I and Case II are represented by circles and squares, respectively. The insets illustrate the position of the region with low electron mobility (shaded area) relative to the cathode (C) and anode (A). Lines are a guide to the eye.

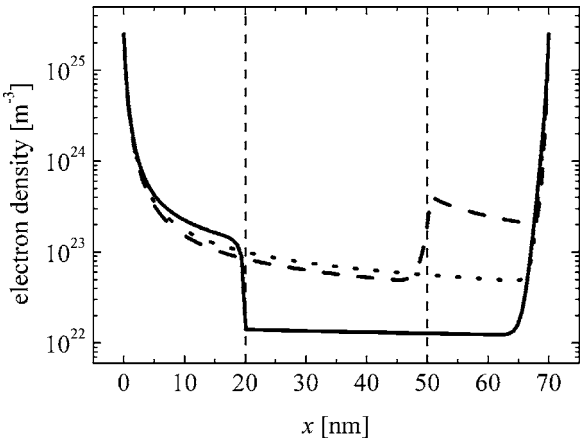

FIG. 3. The electron density as a function of position in the device for Case I (solid line) and Case II (dashed line) for a single-carrier device at +2 V bias. The dotted line corresponds to a single-carrier device with a constant electron mobility. Vertical dashed lines indicate the boundary of the low-mobility layer for the Case I (left) and Case II (right) devices. Both the anode and cathode are assumed to be electron injecting.

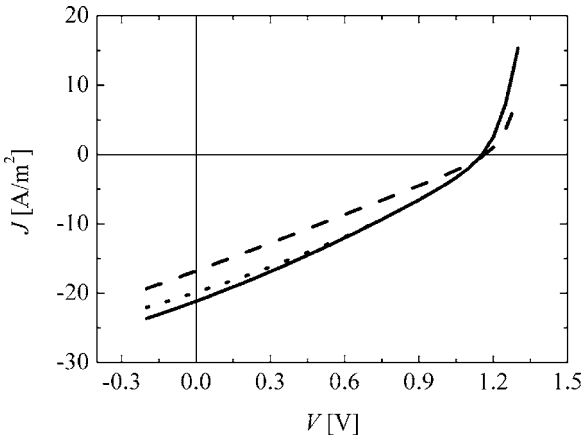

FIG. 4. Simulated current-voltage curves for a device with $z=0$ nm (solid line) and $z=20$ nm in Cases I (dashed line) and II (dotted line).

the Mott–Gurney law is modified to take into account nonuniform mobility, it cannot always be used to correctly interpret data from nonuniform devices.

The difference between the predictions of Eq. (3) and the drift-diffusion model is essentially due to the neglect of diffusion in Eq. (3). In Fig. 3 we show the predictions of the carrier density by the drift-diffusion model for Case I and Case II devices, and a device with uniform mobility for comparison. It can be seen that there is a significant accumulation of charge in the lower mobility regions for both the Case I and Case II devices, and that there is a sharp change in charge density at the boundary between the layers of differing mobility with some "smearing" due to diffusion. The charge density profile around the boundary is only approximately reproduced in the analytical description. This, in turn, leads to a redistribution of the field, which gives rise to an increased drift current for Case I and Case II devices. Hence it is the boundary between the two layers of differing mobility that gives rise to the difference between the analytical and drift-diffusion models.

IV. MOBILITY VARIATIONS IN PV DEVICES

Now we examine what the implications of nonuniform mobility are upon PV device performance. In these double-carrier devices we insert a layer with low electron mobility in the same manner as in Sec. III, while the hole mobility is assumed to be constant throughout the device. Parameters used in the simulation are shown in Table II. Field-dependent geminate recombination efficiency is included after the model of Braun, in a similar manner to previous models.[24] Bimolecular recombination is also included using the Langevin expression for the rate constant, which has recently been shown to be accurate to within an order of magnitude for blend devices [with the notable exception of annealed poly(3-hexylthiophene) (P3HT): 1-(3-methoxycarbonyl) propyl-1phenyl-[6,6]-methanofullerene (PCBM) devices].[25] We assume a uniform generation rate of free charge carriers of 5×10^{27} m^{-3} s^{-1}, which is typical for PV operating conditions. Parameters are shown in Table II.

Figure 4 shows the J-V characteristics of a PV device with no low-mobility layer (i.e., $z=0$), compared against those for Case I and Case II devices with $z=20$ nm. All devices show approximately the same open-circuit voltage and fill factor. However, they do differ in their short-circuit current, J_{SC}, with Case I having J_{SC} 21% lower than that for $z=0$ case. Note that experimental data[3] suggest that even larger changes in mobility due to morphology variations than assumed here may be possible. As in the SCL diode case, having a low-mobility layer adjacent to the anode (Case II) has a lesser effect. The cause of the change in J_{SC} between the various cases is primarily due to bimolecular recombination losses. Figure 5 shows the bimolecular recombination rate for the Case I and Case II devices compared to a device with no low-mobility layer ($z=0$) at short circuit. It can be seen that the insertion of a layer with low electron mobility close to the cathode significantly increases the bimolecular recombination rate in the region of the low-mobility layer. We can rule out geminate recombination losses being a fac-

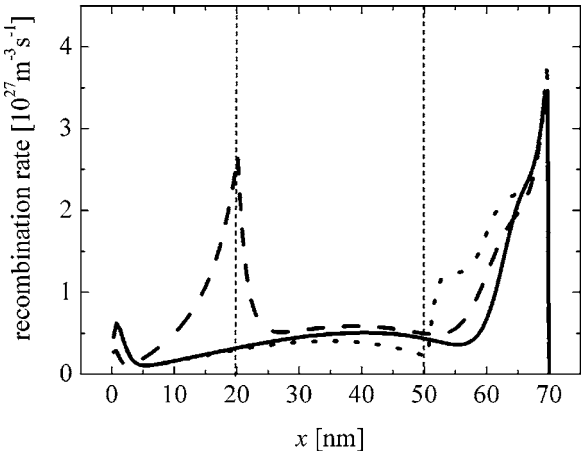

FIG. 5. Recombination rate in the active layer for a device with $z=0$ nm (solid line) and $z=20$ nm in Cases I (dashed line) and II (dotted line). Vertical dashed lines indicate the boundary of the low-mobility layer for the Case I (left) and Case II (right) devices.

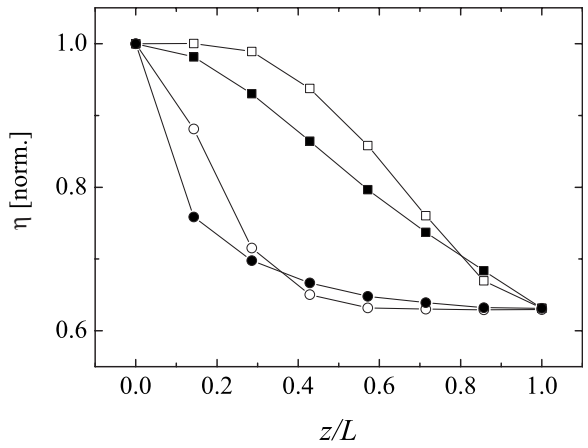

FIG. 6. Simulated power conversion efficiency normalized to the efficiency of a device without a low electron mobility region for Case I (circles) and Case II (squares). Open symbols correspond to the electron mobility exhibiting a jump of a factor of ten, while the closed symbols denote the results for taking the electron mobility constant and equal to $\mu_{e,\mathrm{eff}}$. Lines are a guide to the eye.

tor as the total geminate recombination probabilities are almost identical in the Case I and Case II devices.

The power conversion efficiency η was calculated as a function of z/L. The open symbols in Fig. 6 show the predictions of η for a device with nonuniform electron mobility normalized to the efficiency of a device without any low electron mobility region (i.e., $z=0$). Insertion of a layer with low electron mobility is shown to have a stronger effect in Case I than in Case II. Indeed, insertion of only a 20 nm thick layer with low electron mobility next to the cathode reduces efficiency by ~20%. A consequence of these data would seem to be that it is vital we gain complete control over the blend morphology throughout the entire device, otherwise potential PV performance will be lost.

Since PVs are often analyzed by assuming the device has a uniform blend morphology, it seems pertinent to examine the effect of this assumption if the device has a nonuniform blend morphology. So, in a similar manner to how experimental data are analyzed,[20,21] we now predict the efficiency of a device with a uniform mobility using the effective mobility for a nonuniform device, $\mu_{e,\mathrm{eff}}$ shown in Fig. 2. The data are shown in Fig. 6 as closed symbols, to compare with the open symbols that show the predictions when the mobility is treated as nonuniform. Although relatively small, the differences between the models assuming uniform and nonuniform mobility can be significant when attempting to relate device performance to the underlying materials properties. Larger differences are seen when the variation between mobilities is increased.

V. DISCUSSION AND SUMMARY

Our data show that the range of blend morphologies seen in real PV devices can give rise to significant variations in the local mobility. Of course, the predicted results will not apply to all blend systems. For example, blending poly(2-methoxy-5-(3′,7′-dimethyloctyloxy)-*p*-phenylene vinylene) (OC_1C_{10}-PPV) with PCBM actually improves the transport through the OC_1C_{10}-PPV.[26] Furthermore, blends of P3HT with nonconducting crystalline polymers have been shown to force the P3HT into structures capable of conducting when the concentration of P3HT is only 3 wt %.[27] Whether the present Monte Carlo approach is appropriate depends upon whether the morphologies generated by simulated annealing match the local morphology of the device in question. However, the morphologies used are expected to be accurate for many blends.[14,15,17] Indeed, there is experimental evidence, which shows that the blend morphology can significantly affect mobility in the manner we propose, for example,[28,29] and further data that local morphology affects local charge transport.[8]

Drift-diffusion modeling has shown that changes in the local mobility of one order of magnitude can give rise to significant changes in SCL diode and PV device performance. It is shown that the sequence of the layers with different mobilities makes a profound difference to the current the SCL diode carries, and in turn, the effective mobility derived. Similar behavior is shown in the double-carrier PV device, stressing the need to take into account the morphology of the device when interpreting data taken by experiment. Furthermore it is shown that including layers with a mobility that is reduced by one order of magnitude can reduce the device efficiency by more than 20%. Therefore it is important to exert a high degree of control over the morphology, otherwise potential PV performance may be lost.

ACKNOWLEDGMENTS

The authors would like to acknowledge useful discussions with Dr. C. R. McNeill. This work was supported by the European Commission FP-6 program MODECOM (NMP-CT-2006-016434) and by the Engineering and Physical Sciences Research Council, U.K. This work was performed using the Darwin Supercomputer of the University of Cambridge High Performance Computing Service (http://www.hpc.cam.ac.uk/), provided by Dell Inc. using Strategic Research Infrastructure Funding from the Higher Education Funding Council for England.

APPENDIX: DERIVATION OF EQ. (3)

We first revisit the derivation of the expression for SCL current in the case of a uniform mobility.[30] It is assumed that the current density J is due to drift of electrons of density n,

$$J = e\mu nE. \tag{A1}$$

By combining Eq. (A1) with the Poisson equation, one obtains

$$\frac{dE}{dx} = \frac{J}{\varepsilon\mu E}, \tag{A2}$$

which can be integrated to yield

$$E = \sqrt{\frac{2Jx}{\varepsilon\mu}}, \tag{A3}$$

assuming $E(0)=0$. By integration of Eq. (A3), combined with the boundary conditions $V(0)=0$ and $V(L)=V$, one obtains the Mott–Gurney law

$$J = \frac{9}{8}\varepsilon\mu\frac{V^2}{L^3}. \tag{A4}$$

Equation (3) is derived using similar boundary conditions on the field and the potential at the contacts with the additional constraint that $\mu=\mu_1$ in region 1 $(0<x<z)$ and $\mu=\mu_2$ in region 2 $(x>z)$. Let E_1 and E_2 be the field strength in regions 1 and 2. Similar to Eq. (A3) one has for region 1

$$E_1 = \sqrt{\frac{2Jx}{\varepsilon\mu_1}}, \tag{A5}$$

which implies that the voltage across region 1 is equal to

$$V_1 = \frac{2}{3}z^{3/2}\sqrt{\frac{2J}{\varepsilon\mu_1}}. \tag{A6}$$

For region 2 one has

$$E_2 = \sqrt{\frac{2J(x-z)}{\varepsilon\mu_2}} + C, \tag{A7}$$

where C is a constant of integration. Since the field at $x=z$ is continuous, C is given by

$$C = \sqrt{\frac{2Jz}{\varepsilon\mu_1}}. \tag{A8}$$

Similarly for the potential

$$V(L) = V_1 + \int_z^L E_2(x')dx', \tag{A9}$$

which, by setting the potential to be continuous at $x=z$, can be related to the current density by

$$V = \frac{2}{3}L^{3/2}\sqrt{\frac{2J}{\varepsilon}}\left\{\frac{1}{\sqrt{\mu_1}}\left[\frac{3}{2}\sqrt{\frac{z}{L}} - \frac{1}{2}\left(\frac{z}{L}\right)^{3/2}\right] + \frac{1}{\sqrt{\mu_2}}\left(1-\frac{z}{L}\right)^{3/2}\right\}, \tag{A10}$$

which in turn can be rewritten as

$$J = \frac{9}{8}\varepsilon\mu_{\text{eff}}\frac{V^2}{L^3}, \tag{A11}$$

where μ_{eff} is given by Eq. (3).

[1] J. J. M. Halls, C. A. Walsh, N. C. Greenham, E. A. Marseglia, R. H. Friend, S. C. Moratti, and A. B. Holmes, Nature (London) **376**, 498 (1995).
[2] G. Yu and A. J. Heeger, J. Appl. Phys. **78**, 1540 (1995).
[3] C. R. McNeill, J. J. M. Halls, R. Wilson, G. L. Whiting, S. Berkebile, M. G. Ramsey, R. H. Friend, and N. C. Greenham, Adv. Funct. Mater. **18**, 2309 (2008).
[4] A. C. Arias, J. D. MacKenzie, R. Stevenson, J. J. M. Halls, M. Inbasekaran, E. P. Woo, D. Richards, and R. H. Friend, Macromolecules **34**, 6005 (2001).
[5] A. R. Campbell, J. M. Hodgkiss, S. Westenhoff, I. A. Howrd, R. A. Marsh, C. R. McNeill, R. H. Friend, and N. C. Greenham, Nano Lett. **8**, 3942 (2008).
[6] J.-S. Kim, P. K. H. Ho, C. E. Murphy, and R. H. Friend, Macromolecules **37**, 2861 (2004).
[7] M. Chiesa, L. Burgi, J.-S. Kim, R. Shikler, R. H. Friend, and H. Sirringhaus, Nano Lett. **5**, 559 (2005).
[8] D. C. Coffey, O. G. Reid, D. B. Rodovsky, G. P. Bartholemew, and D. S. Ginger, Nano Lett. **7**, 738 (2007).
[9] H. Hoppe, T. Glatzel, M. Niggemann, W. Schwinger, F. Schaeffler, A. Hinsch, M. Ch. Lux-Steiner, and N. S. Sariciftci, Thin Solid Films **511–512**, 587 (2006).
[10] C. M. Björström, A. Bernasik, J. Rysz, A. Budkowski, S. Nilsson, M. Svensson, M. R. Andersson, K. O. Magnusson, and E. Moons, J. Phys.: Condens. Matter **17**, L529 (2005).
[11] B. Q. Sun, H. J. Snaith, A. S. Dhoot, S. Westenhoff, and N. C. Greenham, J. Appl. Phys. **97**, 014914 (2005).
[12] J. M. Frost, F. Cheynis, S. M. Tuladhar, and J. Nelson, Nano Lett. **6**, 1674 (2006).
[13] A. J. Chatten, S. M. Tuladhar, S. A. Choulis, D. C. Bradley, and J. Nelson, J. Mater. Sci. **40**, 1393 (2005).
[14] R. A. Marsh, C. Groves, and N. C. Greenham, J. Appl. Phys. **101**, 083509 (2007).
[15] P. K. Watkins, A. B. Walker, and G. L. B. Verschoor, Nano Lett. **5**, 1814 (2005).
[16] C. Groves, R. A. Marsh, and N. C. Greenham, J. Chem. Phys. **129**, 114903 (2008).
[17] P. Peumans, S. Uchida, and S. R. Forrest, Nature (London) **425**, 158 (2003).
[18] U. Albrecht and H. Bässler, Chem. Phys. Lett. **235**, 389 (1995).
[19] K. D. Meisel, W. F. Pasveer, J. Cotaar, C. Tanase, R. Coehoorn, P. A. Bobbert, P. W. M. Blom, D. M. de Leeuw, and M. A. J. Michels, Phys. Status Solidi C **3**, 267 (2006).
[20] P. W. M. Blom, M. J. M. de Jong, and J. J. M. Vleggaar, Appl. Phys. Lett. **68**, 3308 (1996).
[21] V. D. Mihailetchi, H. Xie, B. de Boer, L. J. A. Koster, and P. W. M. Blom, Adv. Funct. Mater. **16**, 699 (2006).
[22] S. L. M. van Mensfoort and R. Coehoorn, Phys. Rev. B **78**, 085207 (2008).
[23] B. Crone, P. S. Davids, I. H. Campbell, and D. L. Smith, J. Appl. Phys. **87**, 1974 (2000).
[24] L. J. A. Koster, E. C. P. Smits, V. D. Mihailetchi, and P. W. M. Blom, Phys. Rev. B **72**, 085205 (2005).
[25] C. Groves and N. C. Greenham, Phys. Rev. B **78**, 155205 (2008).
[26] V. D. Mihailetchi, L. J. A. Koster, P. W. M. Blom, C. Melzer, B. de Boer, J. K. van Duren, and R. A. J. Janssen, Adv. Funct. Mater. **15**, 795 (2005).
[27] S. Goffri, C. Müller, N. Stineglin-Stutzmann, D. W. Breiby, C. P. Radano, J. W. Andreasen, R. Thompson, R. A. J. Janssen, M. M. Neilsen, P. Smith, and H. Sirringhaus, Nature Mater. **5**, 950 (2006).
[28] M. Bronner, A. Opitz, and W. Brütting, Phys. Status Solidi A **205**, 549 (2008).
[29] V. D. Mihailetchi, H. Xie, L. J. A. Koster, and P. W. M. Blom, Adv. Funct. Mater. **16**, 699 (2006).
[30] M. A. Lampert and P. Mark, *Current Injection in Solids* (Academic Press, New York, 1970).